# Protein engineering of Pseudomonas fluorescens peroxidase Dyp1B for oxidation of phenolic and polymeric lignin substrates

Pour, R. R., Ehibhatiomhan, A., Huang, Y., Ashley, B., Rashid, G., Mendel Williams, S. & Bugg, T. D. H.

**Author post-print (accepted) deposited by Coventry University's Repository**

# Protein Engineering of *Pseudomonas fluorescens* Peroxidase Dyp1B for Oxidation of Phenolic and Polymeric Lignin Substrates

**Rahman Rahman Pour[1,3], Austine Ehibhatiomhan[2], Yuling Huang[2], Ben Ashley[1], Goran M. Rashid[1], Sharon Mendel-Williams[2] and Timothy D.H. Bugg[1]**

[1]Department of Chemistry, University of Warwick, Coventry CV4 7AL

[2]School of Life Sciences, Coventry University, Coventry CV1 5FB

[3]Department of Bioengineering, University of Illinois at Urbana-Champaign, USA

Author for correspondence: Prof Timothy D.H. Bugg, Department of Chemistry, University of Warwick, Coventry CV4 7AL, U.K. Tel 44-2476-573018 email T.D.Bugg@warwick.ac.uk

**Abstract:**

Directed evolution was applied to dye-decolourizing peroxidase Dyp1B from *Pseudomonas fluorescens* Pf-5, in order to enhance the activity for oxidation of phenolic and lignin substrates. Saturation mutagenesis was used to generate focused libraries at 7 active site residues in the vicinity of the heme cofactor, and the libraries were screened for activity towards 2,6-dichlorophenol. Mutants N193L and H169L were found to show 7-8 fold enhanced $k_{cat}/K_M$ towards DCP, and replacements at Val205 and Ala209 also showed enhanced activity towards alkali Kraft lignin. Residues near the predicted Mn(II) binding site were also investigated by site-directed mutagenesis, and mutants D154E, S223N and H127R showed 4-7-fold increased $k_{cat}/K_M$ for Mn(II) oxidation. Mutant F128R also showed enhanced thermostability, compared to wild-type Dyp1B. Testing of mutants for low molecular weight product release from Protobind alkali lignin revealed that mutant H169L showed enhanced product release, compared with WT enzyme, and the formation of three low molecular weight metabolites by this mutant was detected by reverse phase HPLC analysis.

## Introduction

The dye-decolorizing peroxidases are a family of bacterial and fungal peroxidases, first identified in 1999 [1], that are structurally unrelated to mammalian and plant peroxidases [2], that were initially shown to have high activity for oxidation of anthraquinone dyes [3]. In 2011, *Rhodococcus jostii* RHA1 DypB was first bacterial enzyme to be identified to have activity towards polymeric lignin, a property thought to be held by fungal lignin peroxidases [4]. This enzyme was found to show Mn(II) oxidation activity, which was required for oxidation of polymeric lignin [4]. A multifunctional dye-

decolorizing peroxidase Dyp2 from *Amycolatopsis sp 75iv2* has also been reported to show activity for oxidation of lignin model compounds, and shows much higher Mn(II) oxidation activity than other bacterial DyPs [5]. Amongst Gram-negative bacteria, strains of Pseudomonas have shown activity for lignin oxidation, and a peroxidase Dyp1B from *Pseudomonas fluorescens* Pf-5 has been identified, that shows activity for oxidation of phenolic substrates and, in the presence of Mn(II), polymeric lignin [6]. Uniquely, this enzyme releases an oxidized lignin dimer product from treatment of wheat straw lignocellulose in the presence of Mn(II) [6]. Bacterial DyP-type peroxidases therefore show great potential as biocatalysts for conversion of lignin from industrial processes such as pulp/paper manufacture and biofuel production into renewable chemicals [7,8].

The active site of DyP-type peroxidases contains catalytic aspartic acid and arginine residues that are believed to catalyse formation and stabilization of the compound I iron-oxo reactive intermediate in the catalytic mechanism [2,8]. In *Bjerkandera adusta* DyP, replacement of Asp-171 by Asn leads to a 3,000 fold loss in catalytic activity, consistent with a catalytic role of the bound peroxide ligand [2], whereas in *R. jostii* DypB, replacement of Asp-153 by Ala only slightly reduced the rate of compound I formation, whereas replacement of Arg-244 by Leu led to complete loss of activity [9]. In a *Thermobifida fusca* DyP also shown to have activity for oxidation of Kraft lignin, replacement of Asp-203 by Ala led to a 30-fold loss in $k_{cat}$, while replacement of Arg-315 by Gln led to complete loss of activity [10]. Replacement of a nearby Asn-246 residue in *R. jostii* DypB led to an 80-fold increase in $k_{cat}$ for $Mn^{2+}$ oxidation [11]. The heme pocket of *Auricularia auricular-judae* has been engineered for asymmetric sulfoxidation activity, with a F359G mutant showing up to 99% ee for sulfoxidation of aryl sulfide substrates [12]. Recently, error-prone PCR has been used to engineer a DyP peroxidase from *Pseudomonas putida* MET94 for oxidation of phenolic compounds, with three mutations (E188K, A142V, H125Y) distant from the active site shown to enhance catalytic efficiency for 2,6-dimethoxyphenol by 100-fold [13].

The aim of this study was to enhance activity of *P. fluorescens* Dyp1B for phenolic and polymeric lignin substrate via directed evolution, using the combinatorial active site saturation (CAST) method developed by Reetz *et al* [14]. The strategy employed was to use an initial screen using high redox potential substrate 2,4-dichlorophenol (DCP) which can be monitored spectrophotometrically, and then to use alkali Kraft lignin as a secondary screen, monitoring for increases in absorbance at 465 nm, observed previously for DyP enzymes [4,6]. Since the binding of $Mn^{2+}$ by bacterial DyPs is relatively weak [4,6], we also investigated site-directed mutations at or near the Mn(II) binding site, in order to seek to enhance the activity for Mn(II) oxidation.

**Materials and methods**

### *Homology modelling*

The Swiss-Model webserver [15-19] was used for the homology modelling of the DyP1B protein structure using the FASTA formatted target sequence with UniProt entry number of Q4KAC6_PSEF5. The Crystal structure of *Rhodococcus jostii RHA1* DyPB, (PDB ID 3QNS), was selected as a template. The structural model of the DyP1B protein was obtained in a PDB structure format. The generated model was without any gaps, from amino acid 4 to 283. The Z-score of the model was within the range of scores calculated for proteins of similar size with experimentally determined structures indicating a good overall quality of the built model.

For removing potential steric clashes and suboptimal geometries, the structure was successfully minimized by the AMBER package program [20, 21]. Figure S1 shows the structural model for DyP1B after molecular dynamics. The Z-score of the model was within the range of scores calculated for proteins of similar size with experimentally determined structures.

### *Molecular dynamic simulation*

A 50-ns independent molecular dynamics simulation was performed for the DyP1B homology model. The MD simulation was carried out using the AMBER 12.0 package. The system was solvated by using an octahedral box of TIP3P water molecules with a size of 174.81×153.69×229.20. Periodic boundary conditions and the particle-mesh Ewald method were employed in the simulations [22]. Particle-mesh Ewald method enabled us to calculate the 'infinite' electrostatics without truncating the parameters. During the simulation, all bonds in which the hydrogen atom was present were considered fixed, and all other bonds were constrained to their equilibrium values by applying the SHAKE algorithm [23].

A cut-off radius of non-covalent interactions was set to 12 Å for the protein. The minimization and equilibration phases were performed in two stages. In the first stage, ions and all water molecules were minimized for 500 cycles of steepest descent followed by 500 cycles of conjugate gradient minimization. Afterward, the whole system was minimized for a total of 2500 cycles without restraint wherein 1000 cycles of steepest descent were followed by 1500 cycles of conjugate gradient minimization. In the second stage, the systems were equilibrated for 500 ps while the temperature was raised from 0 to 300 K, and then equilibration was performed without a restraint for 100 ps while the temperature was kept at 300 K. Sampling of reasonable configurations was conducted by running a 50-ns simulation with a 2 fs time step at 300 K and 1 atm pressure. A constant temperature was maintained by applying the Langevin algorithm while the pressure was controlled by the isotropic position

scaling protocol used in AMBER [24]. Time dependence of RMSD (Å) for the backbone atoms relative to the starting structure during 50 ns MD simulation of DyP1B is shown in Figure S2. RMSD curves show that the simulation has reached equilibrium after ~ 30 ns indicated by the relatively stable RMSD values from 30 ns to the end of the simulations.

### *Sequence Alignment and structure observation*

CLC main workbench 6 software was used for protein sequence alignment of DyP1B from *Pseudomonas fluorescens* (UniProt entry number: Q4KAC6), DyP2 from *Amycolatopsis sp* (UniProt entry number: K7N5M8), AauDyP1 from *Auricularia auricula-judae* (UniProt entry number: I2DBY1) and PpDyp from *Pseudomonas putida* (UniProt entry number: Q88HV5). PyMOL software was used for observation of structures of DyP2 (PDB ID 4G2C), AauDyP1(PDB ID 4AU9) and homology model generated structure of DyP1B.

### *Production of libraries by polymerase chain reaction*

For randomizing the selected amino acids, NNK and NDT codons were used for the single and pair sites respectively. NNK codon covers all amino acids codon plus one stop codon whereas NDT codes only 12 amino acids but with a good representation for all amino acid groups. Quick-change II XL site-directed mutagenesis kit was used for introducing the mutations and making libraries. Briefly, PAGE purified primers containing NNK or NDT (Table 4) were used in PCR reactions containing 15 ng DyP1B-TOPO151 plasmid for randomizing each site/s. Except of an increase in the number of PCR cycle to 25, all of PCR conditions and Dpn-I enzyme treatment of PCR reactions were adhered to Quick-change II XL kit protocol. After Dpn-I digestion (2 hours), PCR products were purified using QIAGEN PCR purification kit and subsequently transformed into *E. coli* electrocompetent BL21 (DE3) cells by electroporation. Transformed cells were plated on agar plates containing 100 μg/ml ampicillin and incubated for 14 hours in 37 °C. Plates were kept in 4 °C. For each single site randomization, 96 colonies were picked, and the cells were grown in 700 μl of Luria Bertani media in the presence of ampicillin overnight at 37 °C with 180 rpm shaking in 2ml deep 96 well plates, as a starter culture and glycerol stock for storage in -80 °C. 100 μl of each culture was used to inoculate 700 μl of Luria Bertani broth in the presence of ampicillin and the cells were allowed to grow for four hours in 37 °C with 180 rpm shaking. To each well IPTG and $FeSO_4$ were added in final concentration of 1 mM and 100 μM respectively, and after induction by IPTG the cells were allowed to grow in 20 °C with 180 rpm shaking overnight. The 96 well plates were centrifuged at 4000 rpm for 15 minutes, supernatant was discarded and the cells in the plates were stored at -80 °C. The library quality

was confirmed for each site by sequencing several clones from each library to make sure that the distribution of codons is compatible with the type of degenerate codons used (NNK or NDT) for each site (see Figure S3).

### Screening of libraries for DCP oxidation activity

After two freeze-thawing steps, to each well a 400 µL lysis buffer pH 7.4 containing 50 mM $NaH_2PO_4$, 300 mM NaCl, 0.25% v/v Tween 20 supplemented with 1mg/ml lysozyme, 400 units/ml of DNase type I and 0.5mM PMSF was added. The plates were stirred on an orbital shaker at 37 °C for 60 minutes, then the plates were centrifuged at 4000 rpm for 60 minutes. 2,4-dichlorophenol (DCP) assay was used for screening the generated mutants. The assay was performed in triplicate in 250 µL Nunc plates in 50 mM acetate buffer pH 5.5 at 510 nm. Briefly, each well was containing 3 mM DCP, 0.33 mM 4-aminoantipyrene and 50 µL cleared cell lysate. The reaction was initiated by adding hydrogen peroxide at 1 mM final concentration and monitored for 20 minutes by a Tecan plate reader. Total protein concentration of each cell lysate was measured by Bradford assay in triplicate in 595 nm by a Tecan plate reader.

### Enzyme purification

Protein purification, heme reconstitution and storage for kinetic characterization of the best mutants was performed according to the method previously described in reference 6.

### Kinetic characterization

Kinetic characterization of selected mutants for 2,4-dichlorophenol (DCP) was performed in DCP concentration of 10 µM-6 mM with 1 mM hydrogen peroxide in the presence of 0.18 µM Dyp1B enzyme (engineered or wild type), monitoring at 510 nm ($\varepsilon_{510}$ = 18,000 $M^{-1}cm^{-1}$). Oxidation of alkali Kraft lignin (Sigma-Aldrich) was performed with 50 µM Kraft lignin and 1 mM hydrogen peroxide in the presence of 0.2 µM Dyp1B enzyme (engineered or wild type), monitoring at 465 nm. The molar concentration of Kraft lignin was calculated using an average molecular mass of 10000 Da. Oxidation of $Mn^{2+}$ was carried out using 0.1-6.0 mM $MnCl_2$ in 100 mM sodium tartrate buffer (pH 5.5) in the presence of 1 mM hydrogen peroxide, monitoring at 238 nm ($\varepsilon_{238}$ = 6,500 $M^{-1}cm^{-1}$). Steady state kinetic data (rate vs [S] plots) are shown in Figures S4 (single mutant enzymes) and S5 (multiple mutant enzymes).

### Thermostability

Thermostability of selected mutant was performed in 50 mM acetate buffer pH 5.5, in presence of 3 mM DCP, 0.33 mM 4-aminoantipyrene and 1mM hydrogen peroxide. Briefly, 1 ml of enzyme solution containing 0.075 mg/ml of Dyp1B enzyme in PBS (engineered or wild type) was incubated in 60 °C for 30 minutes and then 100 µl of the enzyme solution was added to 900 µl of the assay buffer, and reaction was initiated by adding hydrogen peroxide.

### Assay for release of ketone products from lignin oxidation

For detecting any released aldehydes or ketones molecules result of reactivity of DyP1B mutants with Lignin, an assay based on reaction of aldehydes with 2, 4-dinitrophenylhydrazine and formation of coloured complex was used [25]. Briefly, 10 µL of Protobind lignin (Green Value Ltd) dissolved in DMSO (25 mg/ml) was added to succinate buffer (1mL, 50 mM, pH 5.5), followed by adding DyP1B (wild type and selected mutant) (100 µL, 1 mg/mL) and hydrogen peroxide (1 mM). The resulting solution was incubated at room temperature for 1 h. Then, 20 µL of solution was mixed with 30 µL HCl (100 mM) followed by adding 50 µL of 2,4-DNP (1 mM dissolved in 100 mM HCl). The mixture was incubated in room temperature for five minutes and then 100 µL NaOH (100 mM) was added and the absorbance was read in 485nm.

### HPLC assay for detection of low molecular weight products

Powdered Protobind lignin (25 mg) was dissolved in DMSO (1 mL), and 30 µL of the sample was added to succinate buffer (3 mL, 50 mM, pH 5.5), followed by addition of DyP1B (wild type or selected mutant) (100 µL, 1 mg/mL) and hydrogen peroxide (1 mM). The resulting solution was incubated at room temperature for 1 h. The reaction was stopped by adding 1M HCl (10 µL), and reaction products were extracted into two volumes of ethyl acetate, and then the solution was centrifuged for 5 min at 10000 rpm. Supernatant was removed, evaporated and the precipitate was dissolved in methanol. HPLC analysis was conducted using a Phenomenex Luna 5 µm $C_{18}$ reverse phase column (100 Å, 50 mm, 4.6 mm) on a Hewlett-Packard Series 1100 analyzer, at a flow rate of 0.5 mL/min, monitoring at 310 nm. The gradient was as follows: 10 to 30% MeOH/$H_2O$ over 10 min, 30 to 40% MeOH/$H_2O$ from 10 to 20 min, 40 to 70% MeOH/$H_2O$ from 20 to 30 min and 70 to 100% MeOH/$H_2O$ from 30 to 40 min.

## Results

*Selection of amino acid residues in Dyp1B for protein engineering*

A homology model of *P. fluorescens* Dyp1B (residues 4-283 of 295 amino acid sequence) was generated from PDB structure 3QNS using the SWISS-MODEL software, followed by 50 nanosecond molecular dynamics energy minimization and structure optimization. Seven amino acid residues positioned around the heme cofactor were selected for saturation mutagenesis using the combinatorial active site saturation (CAST) method developed by Reetz *et al.* [14], on the basis of proximity to the heme cofactor, and sequence alignment, as shown in Figure 1. On the proximal face of the heme cofactor, His169, Val205 and Ala209 were selected. Close to the edge of the heme cofactor, Asn193, Gln165 and Trp167 were selected, while on the distal face of the heme cofactor, Phe218 was selected. The positions of the residues are shown is Figure 1A. Alignment of the sequences of *P. fluorescens* Dyp1B with *P. putida* DyP, *Amycolatopsis* DyP2 and *Auricularia* DyP is shown in Figure 1B, indicating that only Asn-193 is conserved across all four sequences.

Figure 1. Active site of Dyp1B, showing positions of amino acid residues selected for directed evolution. A, active site view; B, amino acid sequence alignment.

*Directed evolution for activity towards DCP & alkali Kraft lignin*

Separate libraries were generated for each amino acid or pair of amino acids noted above. Libraries were screened for activity against 2,4-dichlorophenol (DCP), a high redox potential substrate for which wild type PflDyp1B has relatively low activity [6]. For a single amino acid site, 96 colonies were screened for activity, and for a pair of amino acids, 450 colonies were screened.

Screening of the His169 mutant library gave 7 isolates with >2-fold higher activity than WT enzyme, whose gene sequences were determined. Three mutations were observed: replacement of His by Leu, Val, or Tyr. Specific activities (see Figure 2) were 5-8 fold higher than WT Dyp1B for substrate DCP, with the H169L mutant being the most active mutant. The H169L mutant shows a 3-fold higher $k_{cat}$ than WT Dyp1B, and an 8-fold higher catalytic efficiency (see Table 1). Screening of the Phe218 mutant library also gave 7 isolates with >2-fold higher activity than WT enzyme, which contained replacement of Phe-218 by Pro, Arg, Thr, Ser, Ile, Leu and Gly. Specific activities for five mutants (see Figure 2) were 2-3 fold higher than WT Dyp1B for substrate DCP, with the F218P and F218R mutants being the most active. Both mutants showed similar $k_{cat}$ for DCP, compared to WT Dyp1B, but reduced $K_M$, and F218P shows 2-fold higher catalytic efficiency than WT Dyp1B (see Table 1). Screening of the Asn193 mutant library gave 12 isolates with >2-fold higher activity than WT enzyme. Eight mutations were

observed, containing replacements of Asn-193 by His, Arg, Lys, Leu, Ala, Gly, Tyr and Thr. Specific activities were 1.5-2.5 fold higher than WT Dyp1B for 4 mutants with substrate DCP (see Figure 2), with the N193H and N193L mutants being the most active mutants. Both mutants showed reduced Km for DCP (see Table 1), and mutant N193L shows 8-fold increased catalytic efficiency, compared with WT Dyp1B.

Screening of the Gln165/Trp167 mutant library gave no mutants with higher activity than WT Dyp1B, suggesting that one or both of these residues, which lie close to the edge of the heme cofactor, is important for binding or positioning of the heme cofactor. Screening of the Val205/Ala209 mutant library gave 30-40 mutants with >2-fold higher activity than WT Dyp1B. Determination of the gene sequences gave >25 new sequence variants at these two positions. In position 2015, Ile/Leu/Val was observed most commonly (12 isolates), with Arg or His observed 7 times. In position 209, Asn was observed in 6 isolates, followed by His (4), Leu and Gly (3 each). Testing of 26 isolates against DCP as substrate (see Figure 2) showed that the most active combinations were Ile-His, Val-Asn, Leu-Asn, and Ile-Asn, each with 2.5-fold higher activity than WT Dyp1B. Of these, the V205I/A209H mutant showed highest catalytic efficiency, 4-fold higher than WT Dyp1B (see Table 1).

39 mutants were then re-assayed against alkali Kraft lignin as substrate, monitoring increase at 465 nm versus time, an activity shown previously to exhibit Michaelis-Menten kinetics [6]. As shown in Figure 2B, the pattern of activity against alkali Kraft lignin was rather different to activity for DCP. Whereas replacements at position 169 were most active against DCP, replacements at positions 205/209 were most active against Kraft lignin, with the most active combinations being Leu-His, Val-Cys, Tyr-Asn, His-His, Val-Phe, Val-Leu, and His-Leu.

Table 1 Specific activities of mutants selected by directed evolution

Figure 2 Activities of mutants for DCP vs alkali Kraft lignin

Mutations that gave increased activity were combined to make four mutant enzymes with multiple mutations: two containing mutations with highest activity for Kraft lignin as substrate (P2, V205L/A209H/N193L/H169V/F218G; P3 A209F/N193L/H169V/F218G), and two containing mutations with highest activity for DCP as substrate (P4, V205I/A209H/N193H/H169L/F218P; P5 V205I/A209N/N193H/H169L/F218R), and a further mutant containing a favourable mutation at the $Mn^{2+}$ binding site (P6, V205I/A209H/N193H/H169L/F218P/S223N). Each mutant enzyme was expressed and

purified as above. Assay of the multiple mutant enzymes with DCP as substrate revealed that mutants P3 and P4 showed 2-fold higher $k_{cat}$ that wild-type Dyp1B. Both of these mutant enzymes contained the favourable H169L mutation, and the multiple mutants showed similar kinetic parameters to the H169L single mutant enzyme.

*Screening for thermostability*

Active mutants from libraries at positions 169, 193, and 218 were also tested for thermostability at 60 °C. Mutant F218R was found to exhibit enhanced thermostability, compared with WT Dyp1B, as well as enhanced activity, as shown Figure 3A. F218R was the only mutation at position 218 to show enhanced thermostability, and Phe218 is positioned close to the heme edge (see Figure 3B). A homology model of the F218R mutant suggested that the guanidinium sidechain of Arg could form favourable hydrogen bonds with the heme propionate and with Glu216 (see Figure 3C).

Figure 3. Thermostability of F218R mutant.

*Site-directed mutagenesis of residues at Mn(II) binding site*

Site-directed mutants were also made at residues predicted to be at or near the $Mn^{2+}$ binding site of Dyp1B, in order to improve the binding and catalytic activity for $Mn^{2+}$, which is required for oxidation of polymeric lignin, but is bound relatively weakly by wild-type Dyp1B, with a $K_m$ of 7.3 mM [6]. The Mn(II) binding site determined by X-ray crystallography in *R. jostii* DypB comprises Glu-156, Glu-239, Asp-241 and a heme propionate sidechain [11], however, Asp-241 of *R. jostii* DypB is not conserved in PfDyp1B. The PfDyp1B homology model predicted that His-127 and and Ser-223 might be used as new $Mn^{2+}$ binding residues in this enzyme, as well as Glu-153 and Asp-154. Ser-223 corresponds to Asn-246 in *R. jostii* DypB, whose replacement by Ala is known to cause increase in activity [11].

Figure 4. Predicted Mn(II) binding site for *P. fluorescens* Dyp1B

In order to modify the Mn(II) binding site, each residue was replaced by Ala, and Asp154 was replaced by Glu, His, and Asn,; and Glu153 was replaced by Asp. Ser223 was replaced by Asn (found in RjDypB), and His127 was replaced by Arg (found in RjDypB). The kinetic data for these mutants is shown in Table 2. Mutants D154E, S223N and H127R show 3-4 fold higher $k_{cat}$

9

for oxidation of $Mn^{2+}$, with D154E and H127R showing 7-fold higher $k_{cat}/K_M$ than wild-type Dyp1B. S223N and H127R also show 2-4 fold higher $k_{cat}$ for ABTS oxidation, compared with wild-type Dyp1B. Mutants S223N and H127R were then assayed against alkali Kraft lignin (monitoring changes in absorbance at 465 nm) in the presence of 3 mM MnCl2, and both mutants show 3-4 fold higher rates of lignin oxidation, compared with wild-type Dyp1B (see Table 3).

Table 2. Activities for $Mn^{2+}$ oxidation for site-directed mutants at $Mn^{2+}$ binding site

Table 3. Activity of selected mutants for Kraft lignin oxidation

*Activity against polymeric lignin substrates*

In order to test for the release of low molecular weight products from lignin by Dyp1B mutants, 2,4-dinitrophenylhydrazine was used to detect the release of aldehyde or ketone products, according to a method developed by Tonin *et al* [25]. As shown in Figure 5, wild-type PfDyp1B shows release of some low molecular weight product compared with control, but mutant H169L and multiple mutants P3 and P4 showed 1.5-2 fold higher product release, compared with wild-type PfDyp1B.

Figure 5. Assay of product formation from Protobind alkali lignin using 2,4-dinitrophenylhydrazine

Mutants H169L and V205I/A209N (highest $k_{cat}$ double mutant enzyme) were then incubated with Protobind alkali lignin, and the products analysed by $C_{18}$ reverse phase HPLC. As shown in Figure 6, three peaks were enhanced in size by treatment with mutant enzymes, with greatest product formation by mutant H169L in each case. Both mutant enzymes caused >5 fold enhanced release of a peak 2 at retention time 13 min, compared with WT Dyp1B, which gave *m/z* 165.5 by electrospray mass spectrometry. A possible structure for this product is 4'-hydroxyphenyl-propane-1,2-dione, which could be formed by $\beta,\gamma$-elimination of water from an oxidised triol sidechain observed previously from treatment of wheat straw lignocellulose by wild-type Dyp1B [6]. Peak 1 at retention time 6 min was enhanced by treatment with mutant H169L, and gave *m/z* 159.3 by electrospray mass spectrometry (unidentified structure). Peak 3 at retention time 19 min was enhanced 2-fold by treatment with both mutant enzymes, and

gave *m/z* 175.3 by electrospray mass spectrometry, and was identified as vanillin (MNa$^+$ 175) by comparison with authentic standard.

Figure 6. Analysis by C$_{18}$ reverse phase HPLC of low molecular weight products formed from Protobind alkali lignin by treatment with mutant Dyp1B enzymes.

**Conclusions**

Using a focussed library approach for directed evolution close to the heme binding site of Dyp1B, several mutations have been identified, that show high activity for DCP oxidation. Replacement of His169 by Leu, Val or Tyr leads to increases in activity for DCP, and the H169L mutant shows enhanced product release from Protobind alkali lignin. This residue is found as Asn in *Amycolatopsis* Dyp2 and AuDyP, and is situated close to Trp-167 and Gln-165 for which no active mutants were found, suggesting that the latter residues are important in positioning heme cofactor. Replacement of Asn193, positioned where there is an additional loop in DyP2 and AuDyP, by His, Leu or Lys leads to increased activity for DCP oxidation, but the N193L mutant had little effect on Kraft lignin oxidation or Protobind lignin processing.

Several replacements were found at V205/A209 that showed slightly increased activity for DCP oxidation, but greater activity for Kraft lignin oxidation. Amino acid sequences of DyP2 & AuDyP contain Ile-205, Asn or Arg at position 209, and the optimal sequences for DCP oxidation appear to be V205I and A209H. The V205I/A209H double mutant showed enhanced product release from Protobind lignin.

The different effects of single mutations on activity towards phenolic substrates vs polymeric lignin suggest a different mechanism of oxidation by Dyp1B. It is likely that small molecule substrates such as DCP are bound in the active site close to the heme cofactor, whereas polymeric lignin is oxidised via a surface interaction. A surface residue Trp-377 has been implicated in *Auricularia auricular-judae* dye-decolorizing peroxidase that can form a radical intermediate via long-range electron transfer, for oxidation of bulky dyes [26]. A Recently Brissos *et al* have used error-prone PCR to identify three surface mutations (E188K, A142V, H125Y) in *Pseudomonas putida* MET94 DyP whose replacement gives enhanced activity for DMP substrate [13]. The CAST method for directed evolution focuses on active site residues [15], whereas error-prone PCR is able to identify residues throughout the protein structure, hence it appears that there are residues both near the active site and on the protein surface that contribute towards catalysis in the DyP peroxidase family.

Mutant DyP enzymes with enhanced activity towards lignin substrates are potentially useful for conversion of lignin substrates with recombinant enzyme, either via *in vitro* biotransformation, or via gene overexpression in a lignin-degrading bacterial strain. Future work will therefore investigate the use of such higher activity mutant enzymes for lignin conversion to high value chemicals.

## Acknowledgements

## References

1.  S. J. Kim, M. Shoda, Purification and characterization of a novel peroxidase from *Geotrichum candidum* Dec1 involved in decolorization of dyes. Appl. Environ. Microbiol., 65 (1999) 1029-1035.

2.  Y. Sugano, R. Muramatsu, A. Ichiyanagi, T. Sato, M. Shoda, DyP, a unique dye-decolorizing peroxidase, represents a novel heme peroxidase family. J. Biol. Chem., 282 (2007) 36652-36658.

3.  Y. Sugano, DyP-type peroxidases comprise a novel heme peroxidase family. Cell. Mol. Life Sci., 66 (2009) 1387-1403.

4.  M. Ahmad, J.N. Roberts, E.M. Hardiman, R. Singh, L.D. Eltis, T.D.H. Bugg, Identification of DypB from *Rhodococcus jostii* RHA1 as a lignin peroxidase. Biochemistry, 50 (2011) 5096-5107.

5.  M.E. Brown, T. Barros, M.C.Y. Chang. Identification and characterization of a multifunctional dye peroxidase from a lignin-reactive bacterium. ACS Chem. Biol., 7 (2012) 2074-2081.

6.  R. Rahmanpour, T.D.H. Bugg, Characterisation of Dyp-type peroxidases from *Pseudomonas fluorescens* Pf-5: oxidation of Mn(II) and polymeric lignin by Dyp1B. Arch. Biochem. Biophys., 574 (2015) 93-98.

7.  T.D.H. Bugg, R. Rahmanpour, Enzymatic conversion of lignin into reneable chemicals. Curr. Opin. Chem. Biol., 29 (2015) 10-17.

8. R. Rahmanpour, T.D.H. Bugg, Structure and reactivity of the dye-decolorizing peroxidase (DyP) family. Chapter 14 of "Heme Peroxidases" (eds. E. Raven, B. Dunford), RSC publishing, Cambridge pp. 334-357 (2015).

9. R. Singh, J.C. Grigg, Z. Armstrong, M.E.P. Murphy, L.D. Eltis, The distal heme pocket residues of a B-type dye-decolorizing peroxidase: arginine but not aspartate is essential for peroxidase activity. J. Biol. Chem., 287 (2012) 10623-10630.

10. R. Rahmanpour, D. Rea, S. Jamshidi, V. Fülöp, T.D.H. Bugg, Structure of *Thermobifida fusca* DyP–type peroxidase and activity towards Kraft lignin and lignin model compounds. Arch. Biochem. Biophys., 594 (2016) 54-60.

11. R. Singh, J.C. Grigg, W. Qin, J.F. Kadla, M.E.P. Murphy, L.D. Eltis, Improved manganese-oxidising activity of DypB, a peroxidase from a lignolytic bacterium. ACS Chem. Biol., 8 (2013) 700-706.

12. D. Linde, M. Cañellas, C. Coscolin, I. Davo-Siguero, A. Romero, F. Lucas, F.J. Ruiz-Dueñas, V. Guallar, A.T. Martinez, Asymmetric sulfoxidation by engineering the heme pocket of a dye-decolorizing peroxidase. Catalysis Sci. Technol., 6 (2016) 6277-6285.

13. V. Brissos, D. Tavares, A.C. Sousa, M.P. Robalo, L.O. Martins, Engineering a bacterial DyP-type peroxidase for enhanced oxidation of lignin-related phenolics at alkaline pH. ACS Catalysis, 7 (2017) 3454-3465.

14. M.T. Reetz, M. Bocola, J.D. Carballeira, D. Zha, A. Vogel, Expanding the range of substrate acceptance of enzymes: combinatorial active-site saturation test. Angew Chem Intl Ed 44 (2005) 4192-4198.

15. T. Schwede, J. Kopp, N. Guex, M.C. Peitsch, SWISS-MODEL: An automated protein homology-modeling server. Nucleic Acids Res, 31 (2003) 3381-3385.

16. K. Arnold, L. Bordoli, J. Kopp, T. Schwede, The SWISS-MODEL workspace: a web-based environment for protein structure homology modelling. Bioinformatics 22 (2006) 195-201.

17. N. Guex, M.C. Peitsch, T. Schwede, Automated comparative protein structure modeling with SWISS-MODEL and Swiss-PdbViewer: a historical perspective. Electrophoresis 30 (2009) S162-S173.

18. F. Kiefer, K. Arnold, M. Kunzli, L. Bordoli, T. Schwede, The SWISS-MODEL Repository and associated resources. Nucleic Acids Res 37 (2009) D387-D392.

19. M. Biasini, S. Bienert, A. Waterhouse, K. Arnold, G. Studer, T. Schmidt, F. Kiefer, T. Gallo Cassarino, M. Bertoni, L. Bordoli, T. Schwede, SWISS-MODEL: modelling protein tertiary and quaternary structure using evolutionary information. Nucleic Acids Res 42 (2014) W252-W258.

20. D.A. Case, T.E. Cheatham 3rd, T. Darden, H. Gohlke, R. Luo, K.M. Merz, Jr.; A. Onufriev, C. Simmerling, B. Wang, R.J. Woods, The Amber biomolecular simulation programs. J Comput Chem, 26 (2005) 1668-1688.

21. D.A. Case, T.A. Darden, T.E. Cheatham, C.L. Simmerling, J. Wang, R.E. Duke, R. Luo, R.C. Walker, W. Zhang, K.M. Merz, B. Roberts, S. Hayik, A. Roitberg, G. Seabra, J. Swails, A.W. Götz, I. Kolossváry, K.F. Wong, F. Paesani, J. Vanicek, R.M. Wolf, J. Liu, X. Wu, S.R. Brozell, T. Steinbrecher, H. Gohlke, Q. Cai, X. Wang, J. Ye, M-J. Hsieh, G. Cui, D.R. Roe, D.H. Mathews, M.G. Seetin, R. Salomon-Ferrer, C. Sagui, V. Babin, T. Luchko, S. Gusarov, A. Kovalenko, P.A. Kollman, AMBER 12. University of California, San Francisco 2012.

22. T.Y. Darden, D.M. York, G. Lee, L. Pedersen, Particle Mesh Ewald - an N.Log(N) Method for Ewald Sums in Large Systems. J Chem Phys 98 (1993), *98*, 10089-10092.

23. J.P.C. Ryckaert, G. Ciccotti, H.J.C. Berendsen, Numerical-integration of Cartesian equations of motion of a system with constraints - molecular-dynamics of n-alkanes. J Comput Phys 23 (1977) 321-341.

24. D.A. Case, T.E. Cheatham, T. Darden, H. Gohlke, R. Luo, K.M. Merz, A. Onufriev, C. Simmerling, B. Wang, R.J. Woods, The Amber biomolecular simulation programs. J Comput Chem 26 (2005) 1668-1688.

25. F. Tonin, E. Vignali, L. Pollegioni, P. D'Arrigo, E. Rosini. A novel, simple screening method for investigating the properties of lignin oxidative activity. *Enz. Microb. Technol.* 96 (2017) 143–150.

26. D. Linde, R. Pogni, M. Cañellas, F. Lucas, V. Guallar, M. Camillo Baratto, A. Sinicropi, V. Saez-Jimenez, C. Coscolin, A. Romero, F. Javier Modrano, F.J. Ruiz-Dueñas, A.T. Martinez. Catalytic surface radical in dye-decolorizing peroxidase: a computational, spectroscopic and site-directed mutagenesis study. Biochem. J. 466 (2015) 253-262.

Table 1. Activities of selected mutant enzymes from directed evolution against DCP

| Enzyme | $k_{cat}$ ($s^{-1}$) | $K_M$ (mM) | $k_{cat}/K_M$ ($M^{-1}s^{-1}$) |
| --- | --- | --- | --- |

| | | | |
|---|---|---|---|
| WT Dyp1B | 0.63 | 1.2 | 525 |
| | | | |
| N193H | 0.26 | 0.2 | 1,310 |
| N193L | 0.51 | 0.14 | 3,720 |
| H169L | 2.06 | 0.49 | 4,200 |
| F218P | 0.66 | 0.65 | 1,010 |
| F218R | 0.47 | 0.97 | 480 |
| V205I/A209H | 1.08 | 0.52 | 2,070 |
| V205I/A209N | 0.72 | 0.61 | 1,180 |
| V205I/A209Y | 0.57 | 0.42 | 1,350 |
| A209N | 0.66 | 0.65 | 1,010 |
| | | | |
| V205L/A209H/N193L/H169V/F218G | 0.52 | 0.53 | 980 |
| V205I/A209H/N193H/H169L/F218P | 1.02 | 0.26 | 3,930 |
| V205I/A209N/N193H/H169L/F218R | 1.09 | 0.47 | 2,330 |
| A209F/N193L/H169V/F218G | 0.62 | 0.24 | 2,580 |
| V205I/A209H/N193H/H169L/F218P/S223N | 0.18 | 0.72 | 250 |

Table 2. Activities of site-directed mutants at Mn(II) binding site

| Substrate | Mn$^{2+}$ | | | ABTS | | |
|---|---|---|---|---|---|---|
| Enzyme | $k_{cat}$ (s$^{-1}$) | $K_M$ (mM) | $k_{cat}/K_M$ (M$^{-1}$s$^{-1}$) | $k_{cat}$ (s$^{-1}$) | $K_M$ (mM) | $k_{cat}/K_M$ (M$^{-1}$s$^{-1}$) |
| WT Dyp1B | 2.54 | 3.8 | 660 | 23.7 | 0.94 | 23,700 |
| E153A | 1.84 | 12.4 | 150 | 7.2 | 0.64 | 11,000 |
| E153D | 2.68 | 14.0 | 170 | 10.0 | 0.14 | 71,000 |
| D154E | 9.4 | 2.0 | 4.700 | 5.4 | 0.64 | 8,400 |
| D154H | 2.3 | 5.0 | 470 | 0.14 | 1.31 | 110 |
| S223N | 7.6 | 2.7 | 2,800 | 48.4 | 0.26 | 190,000 |
| D230A | 4.6 | 2.8 | 1,600 | 7.0 | 0.96 | 7,200 |
| H127R | 7.7 | 1.76 | 4,400 | 129 | 0.44 | 290,000 |

Table 3. Activity of selected mutants against alkali Kraft lignin (change in absorbance at 465 nm/min)

| Enzyme | Enzyme + lignin | Enzyme + lignin + 3 mM MnCl$_2$ |
|---|---|---|
| Wild type Dyp1B | 0.0248 | 0.036 |
| Mutant S223N | 0.0397 | 0.1085 |
| Mutant H127R | 0.0207 | 0.0893 |

Table 4. PCR primer sequences for directed evolution, containing either NNK or NDT modifications (underlined).

**Phe218 library**

FW-PHE218: CGCCCCGGAAGCC<u>NNK</u>CTCGTGCGTCGCT

REV-PHE218: AGCGACGCACGAG<u>MNN</u>GGCTTCCGGGGCG

**His169 library**

FW-HIS169: CGATCCAGCAATGGCAG<u>NNK</u>GACTTCCAGGGCTTTGC

REV-HIS 169: GCAAAGCCCTGGAAGTC<u>MNN</u>CTGCCATTGCTGGATCG

**Asn193 library**

FW-ASN193: GCGCCTGAGCGAC<u>NNK</u>GAAGAACTGGACGAC

REV-ASN193: GTCGTCCAGTTCTTC<u>MNN</u>GTCGCTCAGGCGC

**Gln165-Trp167 library**

FW-Q165-W167:  TGGCAGTTTTGCCGCGATC<u>NDT</u>CAA<u>NDT</u>CAGCACGACTTCCAGGGC

REV-Q165-W167:  GCCCTGGAAGTCGTGCTG<u>AHN</u>TTG<u>AHN</u>GATCGCGGCAAAACTGCCA

**Val205-Ala209 library**

FW-V205-A209:  GTCTCGGCCCAC<u>NDT</u>AAGCGCACC<u>NDT</u>CAGGAAAGCTTCGCC

REV- V205-A209: GGCGAAGCTTTCCTG<u>AHN</u>GGTGCGCTT<u>AHN</u>GTGGGCCGAGAC

**Figure legends**

Figure 1 Active site residues selected for saturation mutagenesis. A, active site view, drawn using PYMOL software; B, amino acid sequence alignment of *P. fluorescens* Dyp1B, *P. putida* DypB, *Amycolatopsis sp*. Dyp2, and *Auricularia auricular-judae* DyP.

Figure 2 Activity of mutant enzymes against (A) 2,6-dichlorophenol (DCP) (B) alkali Kraft lignin, assessed by absorbance change at 465 nm. Methods described in Materials and Methods.

Figure 3 Thermostability of F218R mutant. A, activity at 60 ºC, compared with wild-type PfDyp1B and other mutant enzymes at Phe-218; B, position of Phe-218 in homology structural model of PfDyp1B; C, predicted structure of arginine residue at position 218, showing additional hydrogen-bonding interactions.

Figure 4. Predicted Mn(II) binding site of PfDyp1B, based on structural homology model.

Figure 5. Formation of low molecular weight products from oxidation of Protobind alkali lignin, using 2,4-ditrophenylhydrazine to detect aldehyde and ketone low molecular weight products (see Materials and Methods).

Figure 6. Products of treatment of Protobind alkali lignin, analysed by reverse phase HPLC.
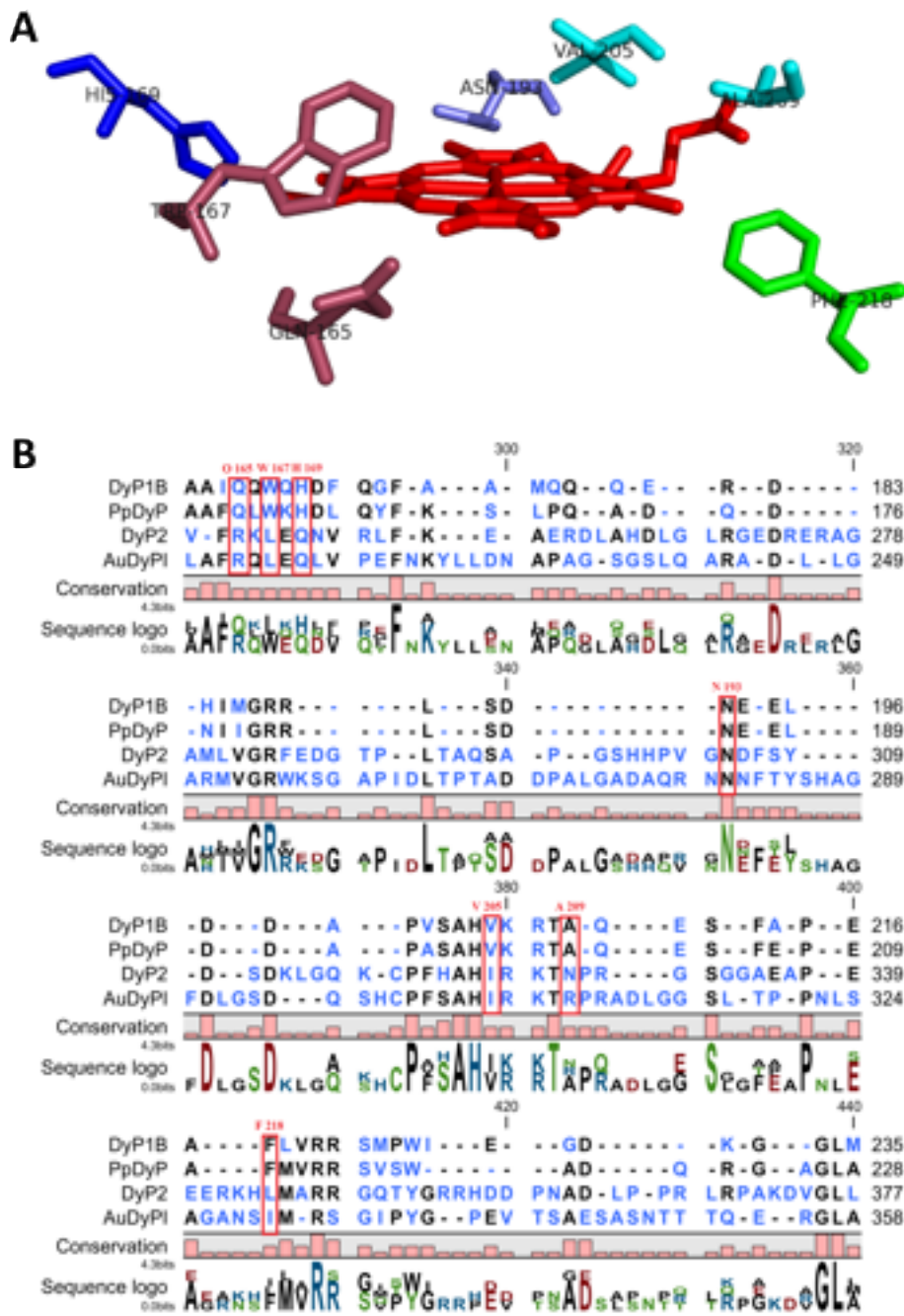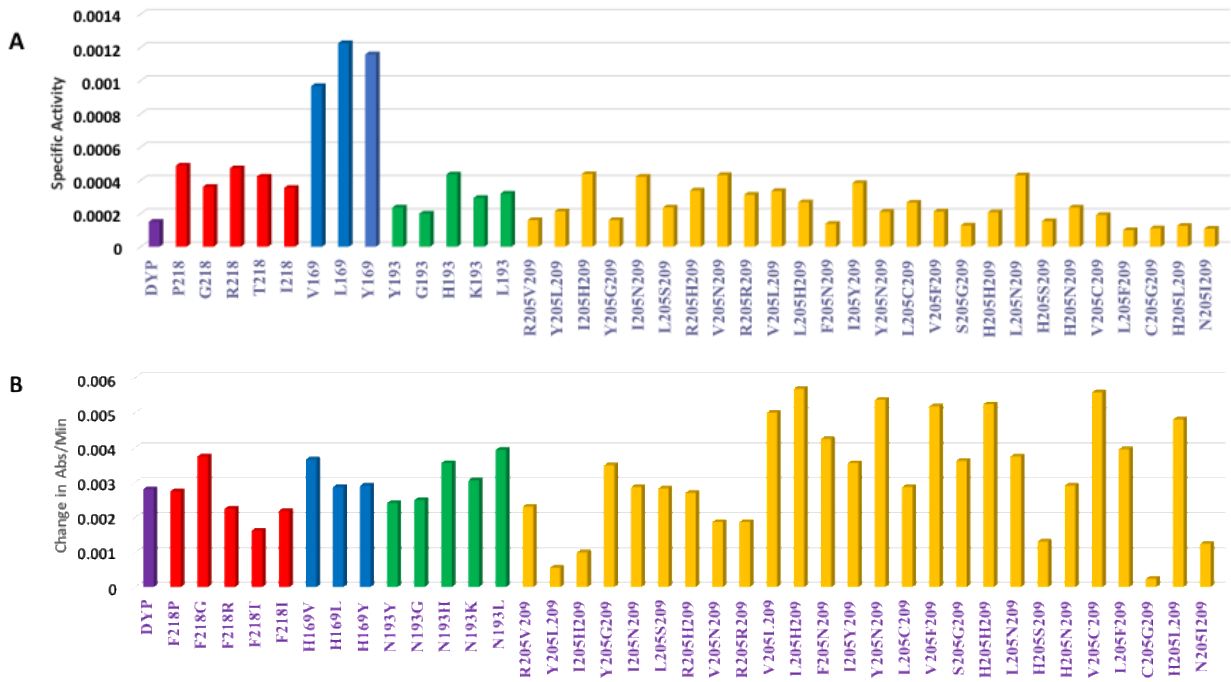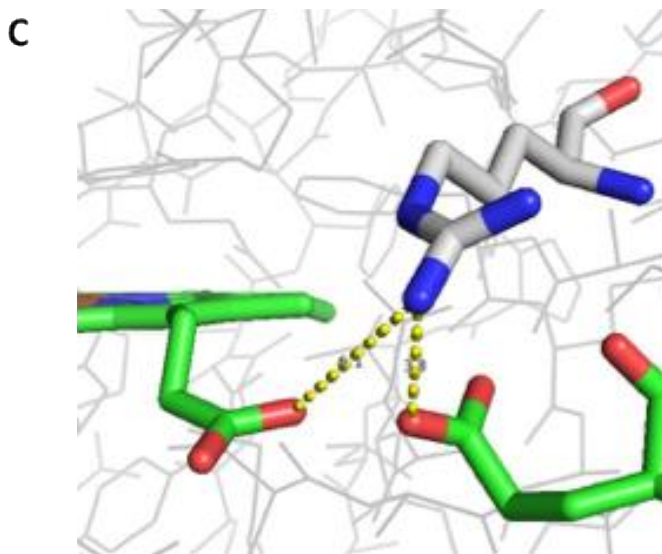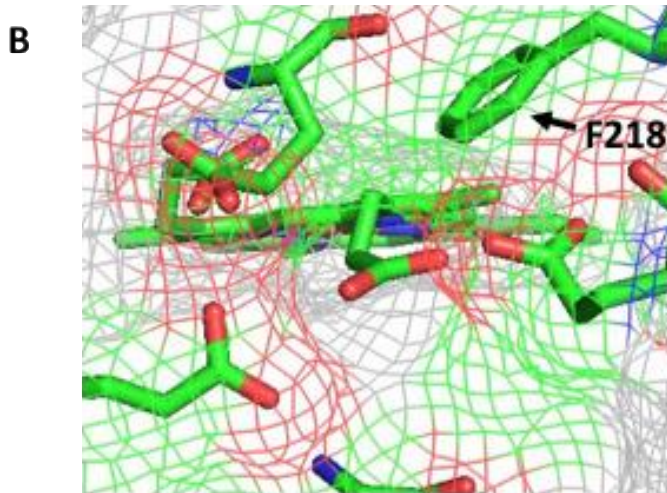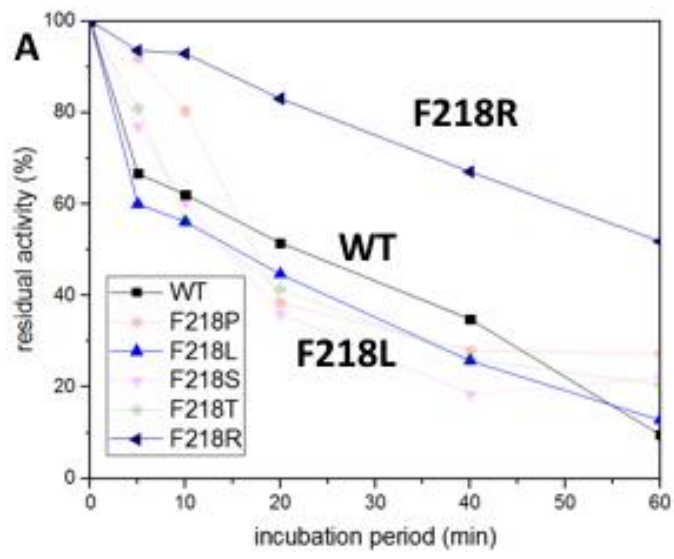
.

Figure 1

Figure 2

Figure 3

Figure 4.



Figure 5.

Figure 6.